European Journal of Agronomy 161 (2024) 127356

Contents lists available at ScienceDirect

European Journal of Agronomy

journal homepage: www.elsevier.com/locate/eja

A custom pipeline for building computational models of plant tissue

Stephen S.B. Clarke [a,b], Alice Benzecry [c], Norbert Bokros [d], Seth DeBolt [d], Daniel J. Robertson [e], Christopher J. Stubbs [a,*]

[a] School of Computer Sciences and Engineering, Fairleigh Dickinson University, NJ, USA
[b] Flight Research Aerospace, CA, USA
[c] Department of Biological Sciences, Fairleigh Dickinson University, NJ, USA
[d] Department of Horticulture, University of Kentucky, KY, USA
[e] Department of Mechanical Engineering, University of Idaho, ID, USA

ARTICLE INFO

Keywords:
Maize
Corn
Stalk
Strength
Lodging
Herbaceous stem
Biomechanics

ABSTRACT

Stalk lodging in the monocot *Zea mays* is an important agricultural issue that requires the development of a genome-to-phenome framework, mechanistically linking intermediate and high-level phenotypes. As part of that effort, tools are needed to enable better mechanistic understanding of the microstructure in herbaceous plants. A method was therefore developed to create finite element models using CT scan data for *Zea mays*. This method represents a pipeline for processing the image stacks and developing the finite element models. 2-dimensional finite element models, 3-dimensional watertight models, and 3-dimensional voxel-based finite element models were developed. The finite element models contain both the cell and cell wall structures that can be tested *in silico* for phenotypes such as structural stiffness and predicted tissue strength. This approach was shown to be successful, and a number of example analyses were presented to demonstrate its usefulness and versatility. This pipeline is important for two reasons: (1) it helps inform which microstructure phenotypes should be investigated to breed for more lodging-resistant stalks, and (2) represents an essential step in the development of a mechanistic hierarchical framework for the genome-to-phenome modeling of herbaceous plant stalk lodging.

1. Introduction

Stalk lodging, defined as the permanent displacement of plants from their vertical orientation, severely reduces agronomic yields of several vital crop species including maize (Berry et al., 2007; Flint-Garcia et al., 2003). Stalk lodging, as opposed to root lodging, occurs when the mechanical stability of the plant is lost due to structural failure of the plant stem (Berry et al., 2004; Robertson et al., 2015). The complex multiscale nature of the stalk lodging phenotype confounds selective breeding studies aimed at reducing stalk lodging (Peiffer et al., 2013; Wang et al., 2024, 2023, 2020; Zhang et al., 2018). For example, high level phenotypes that are strongly correlated with stalk lodging resistance (e.g., strength, and flexural rigidity) are mechanistically linked with lower level intermediate phenotypes like tissue stiffness (Oduntan et al., 2022; Stubbs et al., 2022, 2018; Ookawa et al., 2010). Tissue stiffness is in turn determined by the microstructure and material properties of the cell and cell wall. Complicating this further, cell walls in higher plants are rigid yet extensible structures that vary in their composition between plants, cell types and temporal stages of development (Hofte and Voxeur, 2017). Linking the genome to these lower level intermediate phenotypes, such as microstructure and cell wall stiffness, could enable breeders to alter the high level phenotypes of stalk lodging resistance, strength, and stiffness with more specificity (Prasad and Gupta, 1975; Robertson et al., 2017, 2016; Stubbs et al., 2022; Xue et al., 2020).

Specimen-specific computational models can enable researchers to mechanistically link higher order phenotypes like tissue stiffness to the lower level phenotypes of microstructure and cell wall properties. In particular, sensitivity analysis studies of such computational models can better elucidate the complex nonlinear relationships that exist between microstructure, cell mechanical properties, and tissue stiffness. In this application, finite element models present three distinct advantages:

First, the overall biomechanical responses do not solely depend on the microstructure, but also the material properties of the cell and other factors. Thus, physical experiments that attempt to elucidate the influence of microstructure on tissue stiffness are strongly confounded, and direct comparisons are not practical. However, in silico experiments,

* Corresponding author.
E-mail address: cstubbs@fdu.edu (C.J. Stubbs).

https://doi.org/10.1016/j.eja.2024.127356
Received 29 January 2024; Received in revised form 29 August 2024; Accepted 10 September 2024
Available online 16 September 2024

through the use of finite element modeling, do not have such limitations. In these models, researchers are able to de-couple material properties, morphology, and other factors such as turgor pressure. For instance, by manually assigning the same material properties to all models – as is done in this study – researchers can isolate the cellular morphology and directly compare its influence on the biomechanical response. Similarly, material properties or turgor pressure can be manually changed within a model, and the influence of these factors on tissue stiffness can be directly measured on a per-model basis.

Second, as the models are derived from first principles, the influence measured is mechanistic, not correlational. That is to say, that the results will inform researchers of not just what the impact of individual factors are on tissue stiffness, but will also give insight into how and why.

Third, because individual factors can be isolated, material properties are not required to be known *a priori*. This is because within the linear elastic domain, the stiffness of the finite elements – in this case the cell wall – and the stiffness of the tissue is linear. Thus, to compare microstructures, the material properties of specimens can be manually set to identical, arbitrary values. Furthermore, if researchers wish to determine the material properties of the cell walls, they can use inverse-FEM to solve for them using the microstructure and the overall tissue stiffness. This method is provided in further detail through our previous studies, both as a homogenous structure (Stubbs et al., 2019) or on a per-voxel basis (Stubbs et al., 2020). Such results can be validated against previously developed material tests and plant individual-scale FEM analyses that have already been conducted and are known to simulate lodging with high accuracy (Dupuy et al., 2007; Tomobe et al., 2019; Nakashima et al., 2023).

Unfortunately, the development of specimen-specific finite element models of plant cell microstructure has been to-date impractical and low-throughput. One of the primary challenges to creating these models is transforming imaging data into accurate 3-dimensional models of the plant. For example, the greyscale data produced in micro computed tomography (μCT) scans is often imperfect, and requires researchers to make subjective thresholding decisions or to create specialized processes that may likewise be subjective to create 3-dimensional plant geometries (Bradley and Roth, 2007; Hangartner, 2007; Rulaningtyas and Ain, 2021; Stubbs et al., 2019; Tseng and Huang, 2009; Zhang et al., 2010).

To overcome some of these challenges this paper presents a high-throughput, repeatable, and reliable methodology of building finite element models for *Zea mays* specimens and other commercially important herbaceous crops. Specifically, this method uses a custom pipeline to efficiently convert μCT scans into semi-parameterized specimen-specific finite element models.

Thus, this study presents the pipeline, provides the results of the process, and validates and compares the pipeline based on the current state-of-the-science methods. Additionally, example use cases of 2-dimensional and 3-dimensional finite element models are presented in the Discussion solely to demonstrate the potential utility of the process. As such, this study represents an incremental step in the direction of mechanistically linking microstructure to tissue stiffness and, ultimately, stalk lodging resistance.

2. Methods

2.1. Plant materials

Experimental stalks were collected from border rows within a larger experiment located on the University of Kentucky Spindletop Research Farm. Seed was sourced from a single bag of Pioneer P1464AML (mid-season, 114 days to mature), hand planted on 05/14/2021 and fully mature stalks were harvested around 09/09/2021, approximately 118 days after planting. Immediately before planting, the field was rototilled and a precision planter was used to pre-cut 2-inch deep furrows with 30-inch row-to-row spacing. Planting density was set to 0.1 m/seed within border rows. Weeds were controlled with a single 583 L/km^2 treatment of Acuron supplemented with 16,812 kg/km^2 of nitrogen applied on 06/01/2021. After herbicidal activity wore off, weeds were controlled manually with hoeing as needed; neither supplemental irrigation nor pesticide treatments were required during the growing season. During stalk collection, individuals were cut from the ground at their base using garden shears and at the internode above the primary ear bearing node. All leaves, and leaf sheaths were removed from individual stalks. Stalks were spread in a single layer on wire rack benchtops in a greenhouse set to 36°C w/ adequate air circulation to deter mold growth and allowed to dry for one month. After drying, stalks were cut into subsections of approximately 3 internodes before shipment to University of Idaho, where they were stored at standard office temperature and humidity.

2.2. Specimen preparation & computed tomography scanning

The samples were sectioned using a 110 V, 15.25 cm trim saw with a thin-notched diamond saw blade using the methodology outlined by Oduntan (Oduntan et al., 2022). Samples were then shipped to Micro Photonics (Allentown, PA, USA) for microCT imaging. The samples were soaked in a 1 % aq solution of osmium tetroxide for one week, and then scanned using the SkyScan 1272 with a 70 kV source voltage, 142μA source current, 1238 ms exposure time, and a 0.5 mm Aluminum filter. Scans took approximately three hours per sample, and resulted in a voxel resolution of 4.3μm.

2.3. Processing

2.3.1. Image thresholding

Thresholding (also referred to as binarization) is a common digital image processing technique which converts a grayscale image into one that only contains black and white pixels (Gonzalez, 2009). After thresholding white pixels can be turned into 3D geometries, whereas black pixels represent empty space or gaps between the 3D geometry. Several image processing techniques were utilized in this study to transform grayscale μCT scans into binary images which were in turn made into watertight 3D structures. These techniques included *grayscale erosion*, *otsu thresholding*, *resizing,* and *island-aware erosion*. Each of these are explained in more detail in the following paragraphs.

Grayscale erosion is a grayscale morphology algorithm commonly used in image processing (Serra, 1982). Its aim is to reconstruct an image by iterating over each pixel and calculating the local minimum based on a defined neighborhood. The neighborhood can be defined using any defined structuring element, k. In this study a diamond structuring element was used. This results in an image that is shrunk or contracted, as seen in Fig. 1b. Since the original image is grayscale, many thresholding methods will over-estimate the thickness of the cell wall. Grayscale erosion helps to ensure the thickness of each cell wall is minimal without introducing gaps or holes in the cell walls.

Two-class Otsu Thresholding (Otsu, 1979) with an adaptive window size of 15 pixels was utilized in this study. The results of Otsu Thresholding are shown in Fig. 1 on the top-right. This thresholding algorithm and window size were chosen through experimentation and showed to provide the accurate and representative results. Similar to the previous step, the goal of Otsu Thresholding was to ensure a thin cell wall without introducing gaps or holes in the cell wall.

Next, the image size was doubled in all three axes. This allows for thinner cell walls relative to the entire image size. Island-aware erosion was conducted on the scaled image with the results shown in Fig. 1 on the bottom-right.

Lastly, a custom erosion algorithm was used that is aware of any breaches in the cell wall. During a typical step in an erosion algorithm, a minimum value is calculated within a certain structuring element, k, and will be used as the resulting pixel's value. However, in this custom implementation there is an additional check using a larger and separate structuring element, K, which is used to identify if a cell wall is being breached or not (i.e., if the cell wall is continuous or if it has a hole in it).

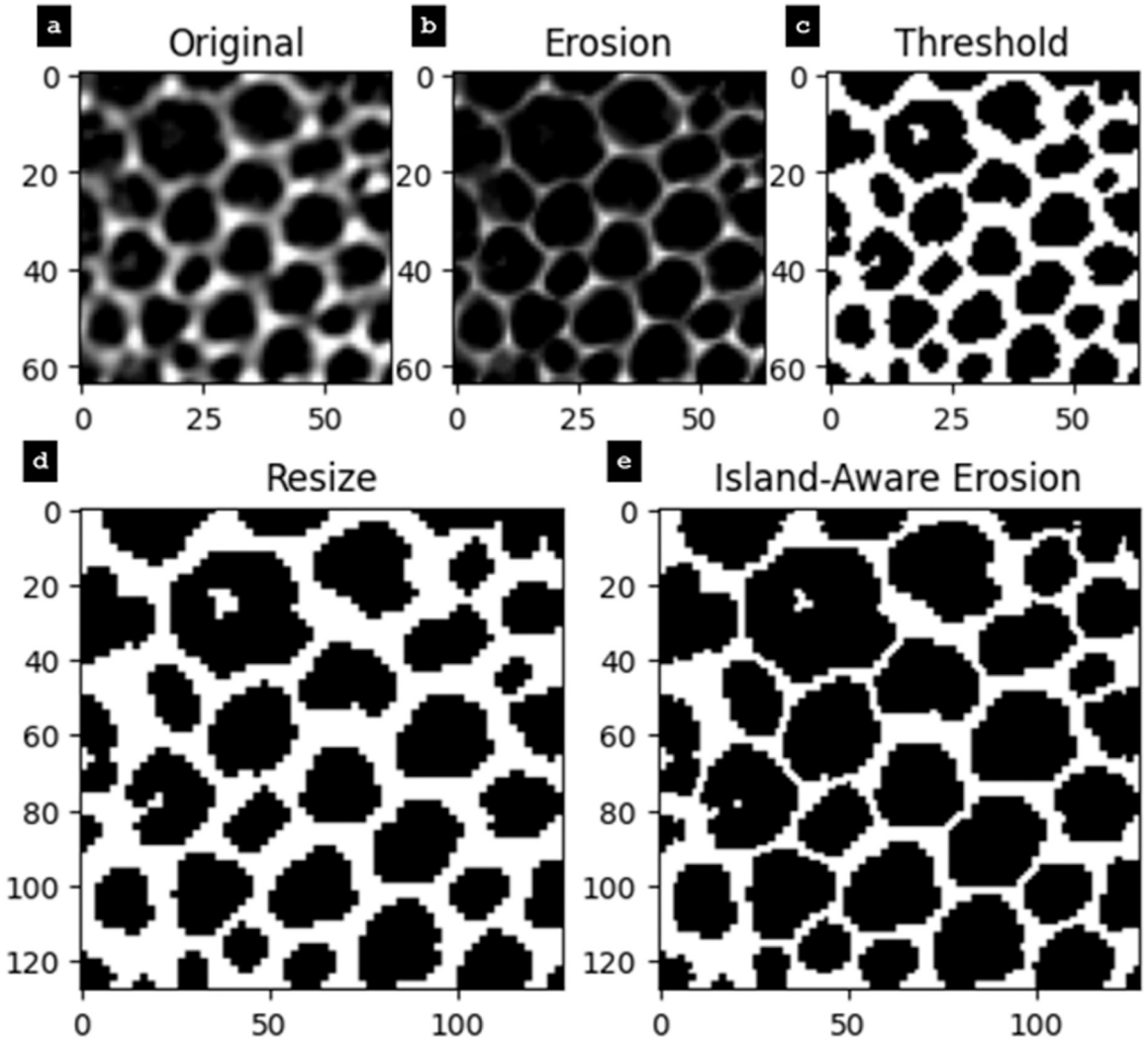

Fig. 1. Image Processing Steps, showing the image at various steps including: the original image (a), the image after the initial erosion step (b), the image after the binary thresholding step (c), the resized image (d), and the image after island-aware erosion (e); voxel size = 4.3μm.

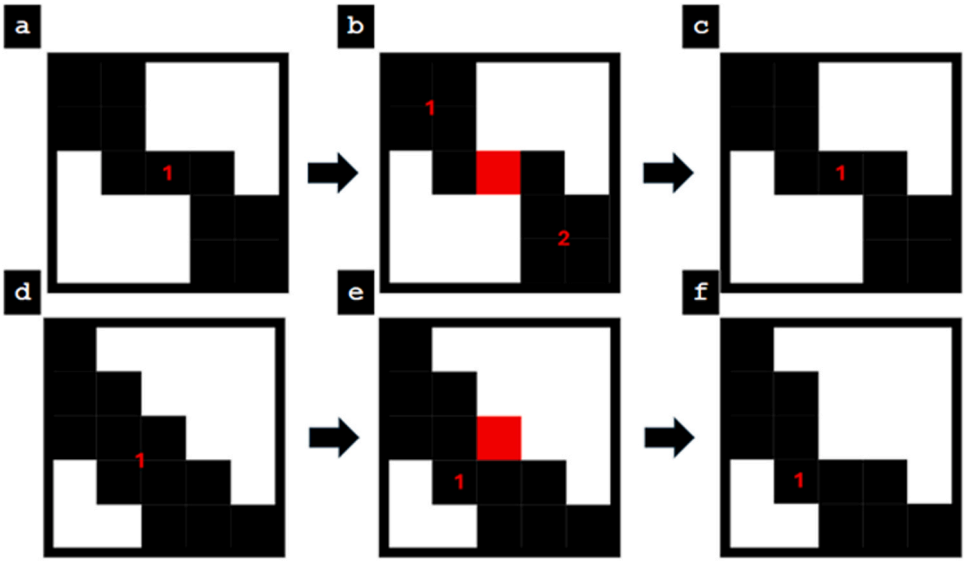

Fig. 2. Island-aware erosion. Top: breach case (a-c). Bottom: no breach (d-f).

If the erosion operation would create a breach of a cell wall, the erosion operation was reversed. To check if a wall is breached, the number of pixel islands are calculated within K before and after a potential erosion operation. If the number of islands is greater after the operation, that implies a breach of a cell wall. This is illustrated in Fig. 2. In the top example, if the center (red) pixel shown in Fig. 2b is removed, then there would be a result of two pixel islands, so we ignore the removal. In the bottom example, an erosion operation would not result in additional islands, so it is performed as normal.

We can see the final resulting image in Fig. 2 on the bottom-right. All code used for image processing and model generation, along with the validation sets discussed in the *Results* section, is uploaded in the GitHub repository: https://github.com/ssbclarke/stalk_cell_segmentation.

3. Results

To evaluate the ability of the μCT scan image processing methodology, validation sets were created and visually compared for performance. To determine good performance, we ensure the final thresholded image reflects the general structure of the original cell wall. This includes representing the relative thickness of the cell wall compared to the entire structure, not introducing holes or breaches in the cell wall, preserving the shape and size of cells, ignoring unwanted noise, and its ability to be reconstructed as a 3D model.

Fig. 3 shows a horizontal cross section of Validation Set #1. Overall, the thresholded image represents the original very well. Two areas of interest are highlighted. First in green on the top-left, notice the breach in the cell wall between two large cells. Although this is representative of the original image which shows the region as dark, in reality these two cells should be separate due to their defined shape, and are shown as disconnected due to localized contrasting. Similarly, in the red area of interest in the bottom-left of the image, there is a breach in the cell wall where there shouldn't be, again due to localized contrasting.

Fig. 4 shows a vertical cross section of Validation Set #2. Here, the thresholded image represents the original well. Looking at the first area of interest in green on the right, we see that there is a gap in the cell wall where the original image contains material. In the red area of interest in the bottom of the image, we see the effect of noise in the original image. Although the inner portion of the highlighted cell is dark in the original, it still contains grayscale information that is determined by the algorithm to be thresholded white. This image also demonstrates good performance in reducing cell wall breaches, as seen in the pink area of interest in the top-left. Although the original image shows a darker gap within the cell wall, the thresholding algorithm correctly fills in the gap.

3.1. Validation & data triangulation

To validate the proposed image thresholding methodology, we compare the results achieved with Otsu thresholding, a technique commonly used for cell segmentation (Mandyartha, 2020; Salem, 2016, Win, 2017). Seen in Fig. 5 panel (c), Otsu thresholding method creates a representative binary image from the original. However, the primary and essential setback occurs within the number of cell wall breaches. In Fig. 5, panel (d), multiple cell wall breaches can be seen in red where the proposed thresholding predicts cell wall, but Otsu thresholding fails to. Limiting these breaches is vital to ensure that the resulting 3D reconstruction is watertight and as representative of the original as possible.

4. Discussion

4.1. Image processing

Through analysis of several segments of our original μCT scanned image we can see that the thresholding process results in an image that is representative of the original structure while being able to be manipulated and converted into a 3D structure. However, it is not without challenges and errors. As seen throughout the validation steps there are areas of improvement such as reducing breaches in cell walls that shouldn't occur, preserving the general shape of each cell and reducing the effect of noise in the thresholded images. Additionally, the thresholding algorithm performs most reliably with higher resolution and less noisy scans. In our results it was found that in regions of small and tightly packed cells, i.e., less resolution per cell, higher error was found in the resulting thresholded image.

4.2. 2-Dimensional finite element model

Two-dimensional finite element analyses of a single slice of a processed image stack can be used in preliminary investigations of microstructure. Although such analyses ignore the variation in the third dimension, they are computational efficient and there results can still be quite informative. To create a 2-dimensional finite element model from a processed *.tiff image stack, the stack is first imported into ImageJ, and the slice of interest is selected and saved as a single image file. Next a custom Matlab code is implemented to trace the cell to cell wall boundaries and write a Python script that sketches the corresponding splines in Abaqus/CAE (Hibbitt et al., 2016; Simulia, 2016). The resulting Python script can then be run in Abaqus/CAE to generate the splines as a sketch. These sketches can then be used to create 2-dimensional finite element parts of the cells and cell walls as separate parts

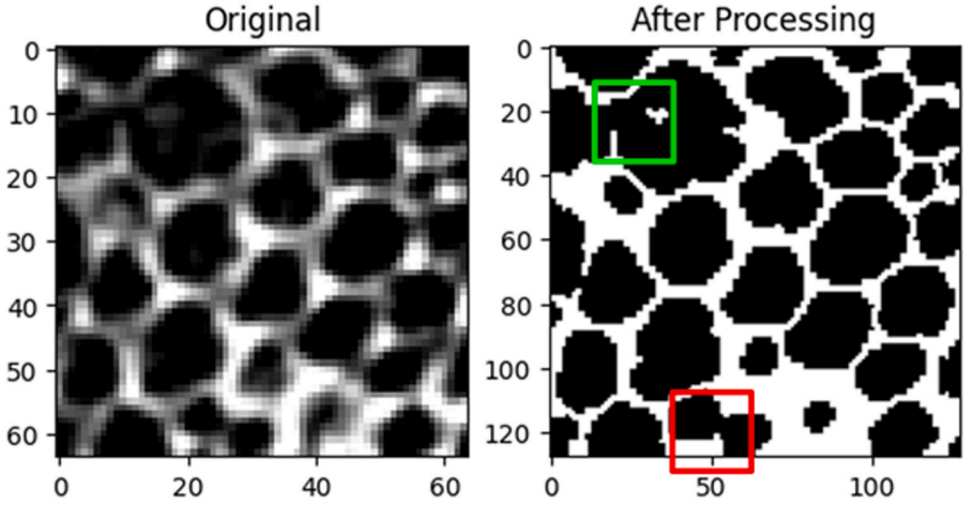

Fig. 3. Image processing validation #1 - horizontal slice. Scale in pixels (voxel size = 4.3μm).

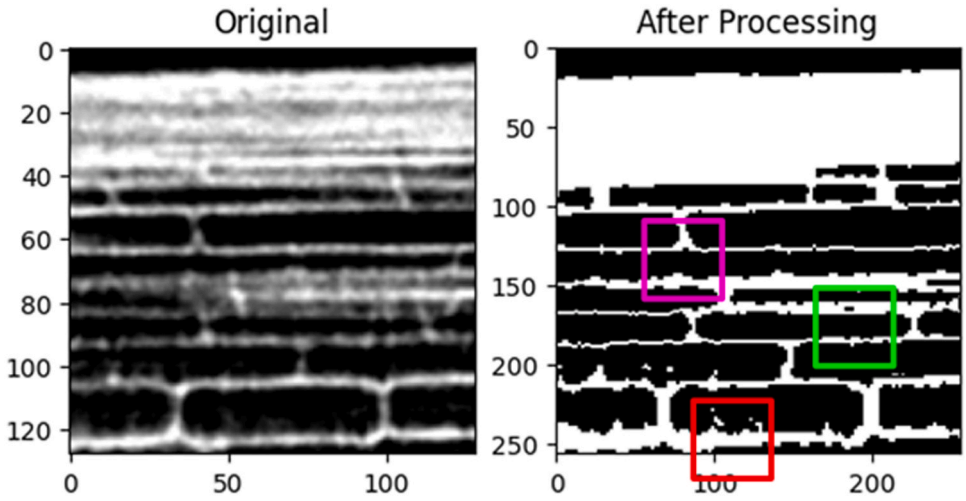

Fig. 4. Image processing validation #2 - vertical slice. Scale in pixels (voxel size = 4.3μm.).

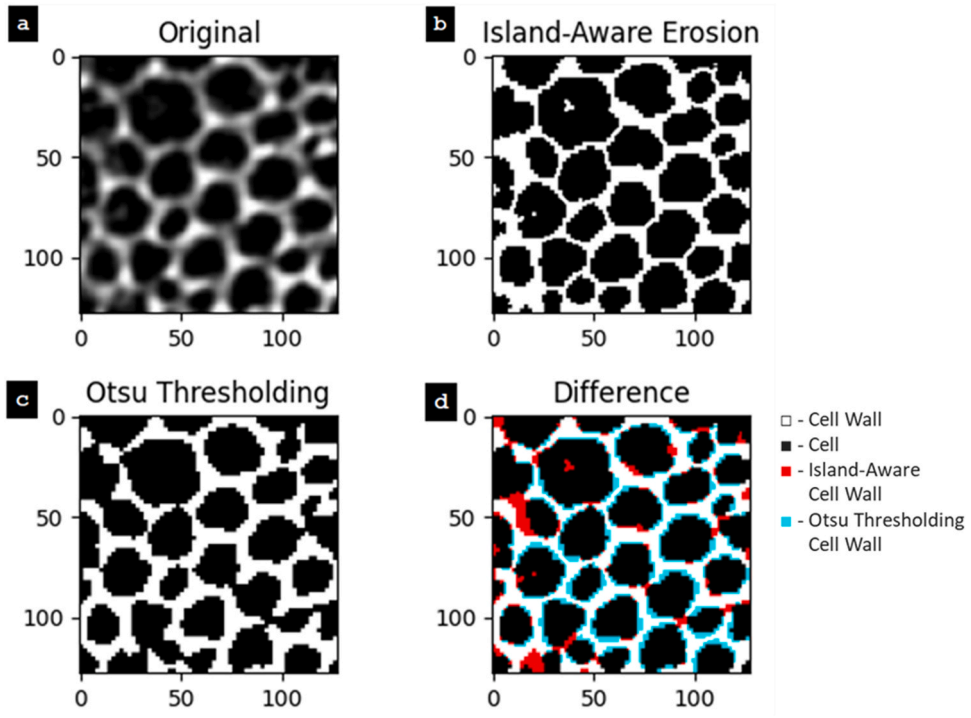

Fig. 5. This image shows our proposed thresholding method using Island-Aware Erosion compared to Otsu thresholding. Shown are four images: (a) the original image, (b) our proposed thresholding using island-aware erosion, (c) Otsu thresholding, and (d) highlights the difference between (b) and (c).

which can be meshed independently and assigned different materials properties. See Fig. 6.

4.3. 3-Dimensional solid model

Although 2-dimensional models can be helpful for initial investigations, it is often necessary to analyze the microstructure as a full 3-dimensional structure. To create such a model, the data needs to be converted into a "watertight" structure; that is to say, we must create a model in which all surfaces combine to define a solid volume. In order to achieve this, we must extract a 3D surface model of the data, and then perform a wrapping function to enclose any open gaps in the volume. To do this, the *.tiff stack is first analyzed in ImageJ using the 3D Viewer plugin, and a surface mesh is extracted. Next, the surface is imported into Meshlab, where a screened Poisson surface reconstruction is performed to ensure the surface is watertight. At this stage, the model is watertight, but contains far more individual faces than are needed; see Fig. 7. Such a large number of faces is a computationally inefficient way to define the volume. Thus, the geometry is simplified using a quadratic edge collapse decimation. An example of this process for one of the samples is shown in Fig. 7. As can be seen, a reduction of the number of faces by over an order of magnitude results in only a relatively minor reduction in the level of detail of the model.

4.4. 3-Dimensional voxel finite element model

At this stage in the process, we have a watertight but hollow surface mesh. Such a mesh can be made solid by importing the model into SolidWorks (SOLIDWORKS 2021) and converting it to a solid using the Surface Thicken tool with "create solid from enclosed volume" enabled.

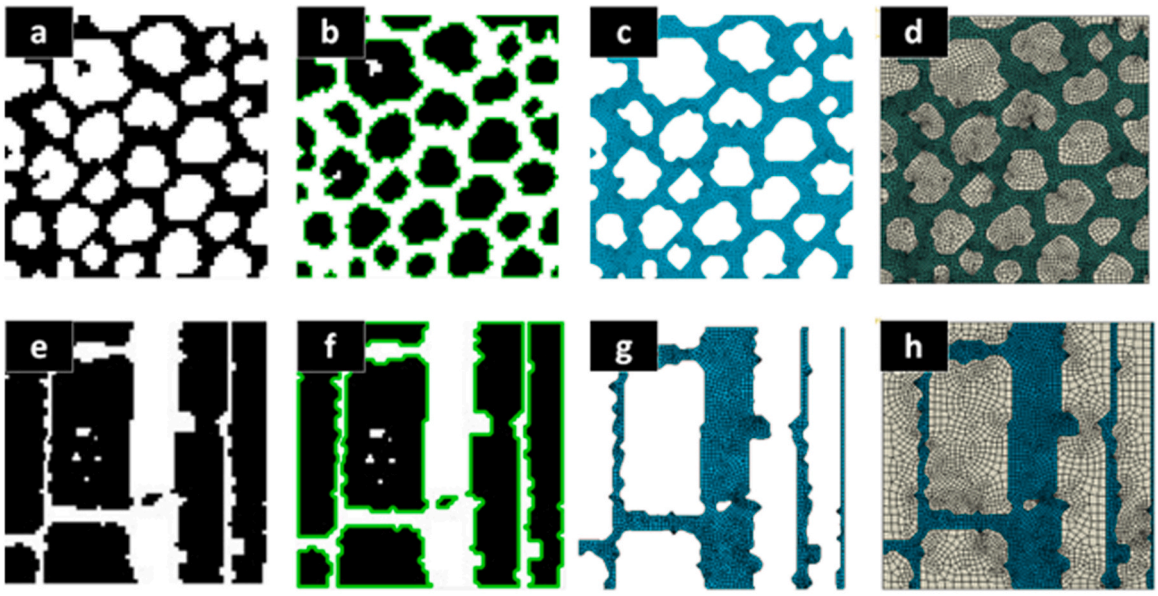

Fig. 6. A single slice of the *.tiff stack resulting from the geometry extraction process (a & e), the tracing of the cell boundaries in MATLAB (b & f), the resulting meshed 2-dimensional finite element model in Abaqus/CAE of the cell walls (c & g), and the final meshed model in Abaqus/CAE with the cells added (d & h); process shown for cross-sectional (top row) and longitudinal (bottom row) slices.

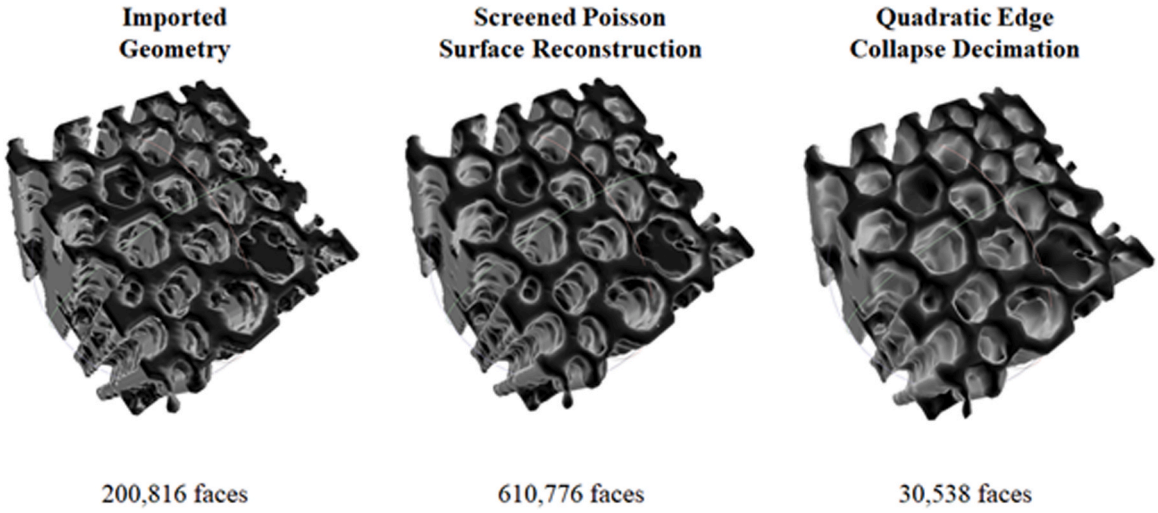

Fig. 7. The mesh processing of the surface geometry in MeshLab, making a single watertight surface that was then simplified to a reduced face count.

However, although this model can be imported into a finite element modeling software like Abaqus/CAE, the resulting geometry is often overly complex and difficult to mesh, even using a free mesh algorithm with quadratic tetrahedral (C3D10) elements, and is quite computational inefficient. In addition, this model only contains cell walls, so we cannot analyze the structure as a cell - wall system. As such, this solid model is often more useful as a tool for volumetric analysis and average bulk tissue density estimates.

Instead, a voxel approach is used to analyze the structure, similar to what has been performed previously in bamboo structures (Palombini et al., 2020). This method uses a standard meshed cube using hexahedral elements, where there is a one-to-one correlation between each element and a corresponding voxel in the processed image stack. Then, each element is assigned material properties corresponding to its position; elements in the position of a cell wall voxel are assigned cell wall material properties, while elements in the position of a cell voxel are assigned cell material properties. In Abaqus/CAE, such mapping of voxels to elements can be done through analytical fields, as we previously presented in (Stubbs et al., 2020).

To demonstrate the feasibility of the voxel mesh approach for evaluating microstructure, a 3-dimensional finite element model was created and analyzed. The model was created as a voxel cube of 64 ×64 x 64 C3D8RT reduced integration temperature-dependent elements, totaling 262,144 elements. The cell and cell wall were mapped using analytical fields, and then analyzed for uniaxial compression in the vertical (y-axis) direction. See Fig. 8.

4.5. Limitations

A number of limitations exist in this process. First, this process has only been tested with CT scans of *Zea mays*. Analyzing different tissue, different species, or different image types would most likely require minor changes to the process. Second, both the image processing and finite element models become exponentially more computationally intensive as the voxel size of the image increases. Key steps like the image erosion or analytical field mapping are key bottlenecks in the

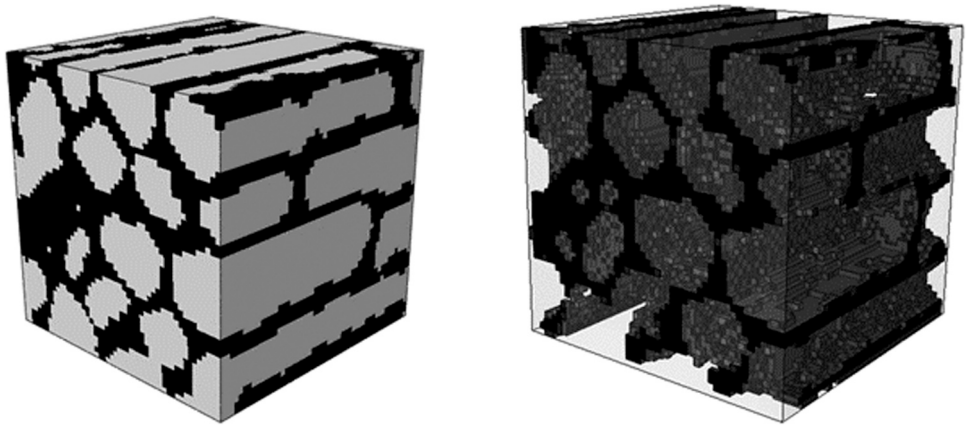

Fig. 8. The resulting voxel model of the cell and cell wall structure, showing the cell wall in black and the cell volumes as white (left) and semi-transparent (right).

process as image sizes become larger. Therefore, computational modeling of entire cross-sections may not be practical.

5. Conclusions

A method was developed to create 2-dimensional and 3-dimensional finite element models using CT scan data for *Zea mays*. This method contains a streamlined pipeline for processing the image stacks and developing the finite element models. 2-dimensional finite element models, 3-dimensional watertight models, and 3-dimensional voxel-based finite element models were developed. The finite element models contain both the cell and cell wall structures. These models can be analyzed for microstructural properties such as force-displacement stiffnesses, as well as be analyzed for stress under different loading conditions.

This approach provides researchers with the tools required to develop a better mechanistic understanding of the microstructure. This is important for two reasons: (1) it helps inform which microstructure phenotypes should be investigated to breed for more lodging-resistant stalks, and (2) represents an essential step in the development of a mechanistic hierarchical framework for the genome-to-phenome modeling of herbaceous plant stalk lodging.

CRediT authorship contribution statement

Daniel J Robertson: Writing – review & editing, Resources, Methodology, Investigation, Funding acquisition, Conceptualization. **Christopher Stubbs:** Writing – review & editing, Writing – original draft, Visualization, Supervision, Resources, Project administration, Methodology, Investigation, Funding acquisition, Formal analysis, Data curation, Conceptualization. **Norbert Bokros:** Writing – review & editing, Resources, Methodology, Investigation. **Seth DeBolt:** Writing – review & editing, Resources, Investigation, Funding acquisition, Conceptualization. **Stephen S B Clarke:** Writing – review & editing, Writing – original draft, Methodology, Investigation, Formal analysis, Conceptualization. **Alice Benzecry:** Writing – review & editing, Conceptualization.

Declaration of Competing Interest

The authors declare that they have no known competing financial interests or personal relationships that could have appeared to influence the work reported in this paper.

Data availability

Data will be made available on request.

Acknowledgements

This work was funded in part by the National Science Foundation (Award #1826715 and #2225211). Any opinions, findings, conclusions, or recommendations are those of the author(s) and do not necessarily reflect the view of the funding bodies.

References

Berry, P., Sylvester-Bradley, R., Berry, S., 2007. Ideotype design for lodging-resistant wheat. Euphytica 154, 165–179. https://doi.org/10.1007/s10681-006-9284-3.

Berry, P.M., Sterling, M., Spink, J.H., Baker, C.J., Sylvester-Bradley, R., Mooney, S.J., Tams, A.R., Ennos, A.R., 2004. Understanding and Reducing Lodging in Cereals. In: Donald, L.S. (Ed.), Advances in Agronomy. Academic Press, pp. 217–271.

Bradley, D., Roth, G., 2007. Adaptive thresholding using integral image. J. Graph. Tools 12, 13–21. https://doi.org/10.1080/2151237X.2007.10129236.

Dupuy, L.X., Fourcaud, T., Lac, P., Stokes, A., 2007. A generic 3D finite element model of tree anchorage integrating soil mechanics and real root system architecture. Am. J. Bot. 94, 1506–1514.

Flint-Garcia, S.A., Darrah, L.L., McMullen, M.D., Hibbard, B.E., 2003. Phenotypic versus marker-assisted selection for stalk strength and second-generation European corn borer resistance in maize. Theor. Appl. Genet. 107, 1331–1336. https://doi.org/10.1007/s00122-003-1387-9.

Gonzalez, R.C., 2009. Digital image processing. Pearson education india.

Hangartner, T.N., 2007. Thresholding technique for accurate analysis of density and geometry in QCT, pQCT and muCT images. J. Musculoskelet. Neuron Interact. 7, 9.

Hibbitt, K., Karlsson, B.I., Sorenson, E.P., 2016. ABAQUS/Standard theory manual. Sorenson Inc.

Mandyartha, E.P., Anggraeny, F.T., Muttaqin, F., Akbar, F.A., 2020. Global and adaptive thresholding technique for white blood cell image segmentation (July). In: In Journal of Physics: Conference Series, Vol. 1569. IOP Publishing, 022054 (July).

Nakashima, T., Tomobe, H., Morigaki, T., Yang, M., Yamaguchi, H., Kato, Y., Guo, W., Sharma, V., Kimura, H., Morikawa, H., 2023. Non destructive high throughput measurement of elastic viscous properties of maize using a novel ultra micro sensor array and numerical validation. Sci. Rep. 1–12.

Oduntan, Y.A., Stubbs, C.J., Robertson, D.J., 2022. High throughput phenotyping of cross-sectional morphology to assess stalk lodging resistance. Plant Methods 18 (1). https://doi.org/10.1186/s13007-021-00833-3.

Ookawa, Taiichiro, et al., 2010. New approach for rice improvement using a pleiotropic QTL gene for lodging resistance and yield. Nat. Commun. 1 (1), 132.

Otsu, N., 1979. A threshold selection method from gray-level histograms. IEEE Trans. Syst. Man Cybern. 9, 62–66. https://doi.org/10.1109/TSMC.1979.4310076.

Palombini, F.L., Lautert, E.L., Mariath, J.E., de, A., de Oliveira, B.F., 2020. Combining numerical models and discretizing methods in the analysis of bamboo parenchyma using finite element analysis based on X-ray microtomography. Wood Sci. Technol. 54, 161–186.

Peiffer, J.A., Flint-Garcia, S.A., De Leon, N., McMullen, M.D., Kaeppler, S.M., Buckler, E. S., 2013. The genetic architecture of maize stalk strength. Plos One 8 https://doi.org/ARTN e67066 10.1371/journal.pone.0067066.

Prasad, J., Gupta, C.P., 1975. Mechanical properties of maize stalk as related to harvesting. J. Agric. Eng. Res. 20, 79–87. https://doi.org/10.1016/0021-8634(75)90098-0.

Robertson, D.J., Julias, M., Lee, S.Y., Cook, D.D., 2017. Maize stalk lodging: morphological determinants of stalk strength. Crop Sci. 57, 926–934. https://doi.org/10.2135/cropsci2016.07.0569.

Robertson, D.J., Lee, S.Y., Julias, M., Cook, D.D., 2016. Maize stalk lodging: flexural stiffness predicts strength. Crop Sci. 56, 1711. https://doi.org/10.2135/cropsci2015.11.0665.

Robertson, D.J., Smith, S.L., Cook, D.D., 2015. On measuring the bending strength of septate grass stems. Am. J. Bot. 102, 5–11. https://doi.org/10.3732/ajb.1400183.

Rulaningtyas, R., Ain, K., 2021. CT scan image segmentation based on hounsfield unit values using Otsu thresholding method. in: Journal of Physics: Conference Series. IOP Publishing, 012080.
Salem, N., Sobhy, N.M., El Dosoky, M., 2016. A comparative study of white blood cells segmentation using otsu threshold and watershed transformation. J. Biomed. Eng. Med. Imaging 3 (3), 15.
Serra, J., 1982. Image analysis and mathematical morphol-ogy. No Title.
Simulia, D.S., 2016. ABAQUS Analysis Manual. Provid. RI.
Stubbs, C.J., Baban, N.S., Robertson, D.J., Al-Zube, L., Cook, D.D., 2018. Bending Stress in Plant Stems: Models and Assumptions. In: Geitmann, A., Gril, J. (Eds.), Plant Biomechanics - From structure to function at multiple scales. Springer Verlag, pp. 49–77.
Stubbs, C.J., Larson, R., Cook, D.D., 2022. Maize stalk stiffness and strength are primarily determined by morphological factors. Sci. Rep. 12, 1–11. https://doi.org/10.1038/s41598-021-04114-w.
Stubbs, C.J., Larson, R., Cook, D.D., 2020. Mapping spatially distributed material properties in finite element models of plant tissue using computed tomography. Biosyst. Eng. 200, 391–399. https://doi.org/10.1016/j.biosystemseng.2020.10.008.
Stubbs, C.J., Sun, W., Cook, D.D., 2019. Measuring the transverse Young's modulus of maize rind and pith tissues. J. Biomech. 84, 113–120. https://doi.org/10.1016/j.jbiomech.2018.12.028.
Tomobe, H., Fujisawa, K., Murakami, A., 2019. Experiments and FE-analysis of 2-D root-soil contact problems based on node-to-segment approach. Soils Found. 59, 1860–1874.
Tseng, L.-Y., Huang, L.-C., 2009. An adaptive thresholding method for automatic lung segmentation in CT images. in: AFRICON 2009. IEEE, pp. 1–5.
Wang, B., Yang, M., Guo, H., Wang, J., Wang, Z., Lu, H., Qin, G., Chen, J., 2024. Genome-wide association study for stalk lodging resistance related traits in maize (Zea mays L.). BMC Genom. 25, 19.
Wang, S., Li, H., Dong, Z., Wang, C., Wei, X., Long, Y., Wan, X., 2023. Genetic structure and molecular mechanism underlying the stalk lodging traits in maize (Zea mays L.). Comput. Struct. Biotechnol. J. 21, 485–494.
Wang, X., Shi, Z., Zhang, R., Sun, X., Wang, J., Wang, S., Zhang, Y., Zhao, Y., Su, A., Li, C., 2020. Stalk architecture, cell wall composition, and QTL underlying high stalk flexibility for improved lodging resistance in maize. BMC Plant Biol. 20, 1–12.
Win, K.Y., Choomchuay, S., 2017. Automated segmentation of cell nuclei in cytology pleural fluid images using OTSU thresholding (March). In 2017 International Conference on Digital Arts, Media and Technology (ICDAMT). IEEE, pp. 14–18 (March).
Xue, J., Gao, S., Fan, Y., Li, L., Ming, B., Wang, K., Xie, R., Hou, P., Li, S., 2020. Traits of plant morphology, stalk mechanical strength, and biomass accumulation in the selection of lodging-resistant maize cultivars. Eur. J. Agron. 117, 126073.
Zhang, J., Yan, C.-H., Chui, C.-K., Ong, S.-H., 2010. Fast segmentation of bone in CT images using 3D adaptive thresholding. Comput. Biol. Med. 40, 231–236.
Zhang, Y., Liu, P., Zhang, X., Zheng, Q., Chen, M., Ge, F., Li, Z., Sun, W., Guan, Z., Liang, T., 2018. Multi-locus genome-wide association study reveals the genetic architecture of stalk lodging resistance-related traits in maize. Front. Plant Sci. 9, 611.